Tanzania Journal of Science 44(2): 16-26, 2018 ISSN 0856-1761, e-ISSN 2507-7961

IN VIVO ANTIMYCOBACTERIAL STUDIES OF TOUSSAINTINE A-CHITOSAN NANOCOMPOSITES

Edward Rwegasila[1], Joan JE Munissi[1*], Egid B Mubofu[1], Stephen S Nyandoro[1] and Paul Erasto[2]

1 Chemistry Department, College of Natural and Applied Sciences, University of Dar es Salaam, P.O. Box 35061, Dar es Salaam, Tanzania

2 National Institute for Medical Research (NIMR), P.O. Box 9653, Dar es Salaam, Tanzania

*****Correspondence: joan.munissi@udsm.ac.tz

ABSTRACT

Chitosan (CS, molecular weight (MW) 20.2 kDA, stability of 210 °C and degree of deacetylation (DD) 73.31%) was obtained by deacetylation of chitin extracted from shrimp (Litopenaeus vannamei) shell wastes. The encapsulation of the studied bioactive natural product, toussaintine A (TA) isolated from the leaves of Toussaintia orientalis, on a chitosan-tripolyphosphate (CS/TPP) nanoformulation was attained through ionotropic gelation. Characterization of pure CS, CS/TPP and TA-CS/TPP nanocomposites was carried out by FTIR and SEM. The encapsulation efficiency and loading capacity of the TA were 69.33 and 0.46%, respectively. The in vitro release kinetics established an initial release of 27% of TA in the initial six hours followed by a slow and maintained release up to 72 h. The in vivo antimycobacterial acitivities of both TA and TA-CS/TPP nanocomposites against Mycobacterium indicus pranii (MIP) employing Galleria mellonella larvae as an infection model were evaluated. TA-CS/TPP nanocomposite formulations exhibited remarkable effectiveness against MIP than free TA.

Keywords: Toussaintine A; chitosan; nanocomposites, antimycobacterial; *Galleria mellonella*

INTRODUCTION

Nanotechnology is a useful innovation for growing, shaping or assembling of systems either mechanically, chemically or biologically to form nanoscale architectures and devices some of which find their applications in the field of therapeutics through designing various drug delivery systems (Zhang et al. 2008, Ranjita et al. 2011, Da Silva 2013). Applications of nanoparticle-based systems have been reported as drug delivery carriers for treatment and prevention of diseases including tuberculosis (TB). This is due to their ability to intersect biological barriers and target the cellular reservoirs of *Mycobacterium tuberculosis* in addition to their beneficial adjuvant for vaccines (Tiyaboonchai 2003, Ranjita 2011). Biomedical applications of biomaterials such as exosomes, liposomes and chitosan have been extensively investigated for their significant potential. However, with regard to chitosan, much interest has been taken aboard due to its biocompatibility, biodegradability, inexpensiveness, stability, low-toxicity as well as its simple and possible formulation in nanoparticles or in gels, and their cationic properties that influence its antimicrobial activity despite some technological limitations (Tiyaboonchai 2003, Dhillon et al. 2013). Studies on chitosan have demonstrated its potentials as drug agents delivery carriers as proven by the encapsulation of the natural products quercetin, curcumin and panchovillin which have anticancer and anti-TB properties that resulted into enhanced activities compared to the free referred agents (Zhang et al. 2008, Rwegasila et al. 2016). Thus, application of nanotechnology in drug delivery has emerged

as a potential tool for combating the challenges facing the treatment of tuberculosis involving the use of first line anti-tubercular drugs such as rifampicin, isoniazid, ethambutol and pyrazinamide (WHO 2013). The longer treatment periods (approximately six to twelve months), result into development of drug-resistance TB strains and hence seeking alternative versions of treatment using nanostructures to improve drug delivery and bioavailability is vital. Parallel, applicability of natural products has been hindered by various factors including low solubility, poor stability, low bioavailability and lack of target specificity, leading to inaccessibility at their most effective levels at the target site. The present study thus, aimed at investigating the feasibility of encapsulating toussaintine A (TA, Fig. 1) into chitosan nanocomposites to enhance its activity against *Mycobacterium indicus pranii*. TA is among the antitubercular *N*-cinnamoyl tetraketide derivatives (toussaintines) recently isolated from *Toussaintia orientalis* Verdic (Annonaceae) (Samwel 2011, Nyandoro et al. 2015), an extremly endangered plant species endemic to Tanzania (Deroin and Luke 2005, Nyandoro 2014). Toussaintine A was therefore, selected as a representative toussaintines, while *Mycobacterium indicus pranii* (MIP) was chosen as a test *Mycobaterium* species using *Galleria mellonella* larvae as an *in vivo* infection model to study the antimycobacterial properties of the named compound when encapsulated into the chitosan (CS)/tripolyphosphate (TPP) nanoframework.

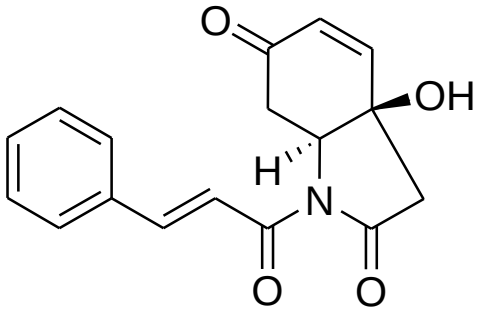

Figure 1: Chemical structure of toussaintine A (TA)

MATERIALS AND METHODS

Test Organisms

The non-pathogenic *Mycobacterium indicus pranii* (MIP) strain DSM 45239 supplied by DSMZ (The Germany Resource Centre for Biological Materials, Braunschweig, Germany) was used to determine anti-mycobacterial properties of the free toussaintine A (TA) and TA-CS/TPP nanocomposites.

Reagents and Other Materials

All chemicals and reagents used were of analytical grade. Chitosan (molecular weight 20.2 kDa, degree of *N*-deacetylation 73.5% and thermal stability of 210 ^{o}C) and the bioactive pure TA (Figure 1) were isolated from chitin and *Toussaintia orientalis*, respectively in previous studies (Nyandoro et al. 2015, Rwegasila et al. 2016). Tripolyphosphate (TPP) was purchased from Sigma-Aldrich (Stockholm, Sweden) and used without further purification.

Preparation of CS/TPP and TA-CS/TPP Nanocomposites

The Chitosan (CS/TPP) nanoformulations and TA-CS/TPP were synthesized through the ionotropic gelation (Calvo et al. 1997, Mohammadpour et al. 2012, Vimal et al. 2013). During formulation, CS was dissolved in acetic acid aqueous solution to afford the concentration of 2 mg/mL (prepared by

dissolving 10 mg of chitosan in 5 mL of acetic acid, while keeping the concentration of acetic acid 1.75 higher than that of chitosan) (Calvo et al. 1997). Moreover, 2 mL of the 1 mg/mL solution of sodium tripolyphosphate (TPP) (prepared by dissolving 2 mg of TPP in 2 mL of distilled water) was added dropwise to 5 mL of chitosan solution while stirring continously at 1000 rpm for 1 h at room temperature (Mohammadpour et al. 2012). This ensued a self-generated fabrication of chitosan colloidal solution. Separation of nanostructured colloidal solution was achieved by centrifugation to afford nanostructured chitosan that was lyophilized, weighed and stored in a refrigerator for further application. The encapsulation of TA to the CS/TPP nanomaterials was carried out using 5:1 CS/TPP mass ratio, the effective CS/TPP ratio ensuing improved encapsulation efficiency as previously established [Rwegasila et al. 2016]. Subsequently, the same 5:1 CS/TPP mass ratio was applied for the *in vitro* release kinetics, the *in vivo* antimycobacterial assay and SEM characterization.

Encapsulation of TA for Bioassay Using Chitosan Solution

Encapsulation of the bioactive molecule, TA adopted the same method described by Rwegasila (2016) in a previous study. In summary, TA-CS/TPP nanocomposites were obtained through the established protocol (Mohammadpour et al. 2012). The resulting TA-CS/TPP nanocomposites were centrifuged at 3500 rpm for 30 min under room temperature. The supernatant containing free toussaintine A was collected and filtered using 125 mm filter paper to acquire a clear solution. The clear supernatant solution was analyzed using the UV-Vis spectrophotometer to quantify the unloaded compound. The nanocomposites collected were mixed with pure water and re-centrifuged. The supernatant obtained was further analyzed using the UV-Vis spectrophotometer for the presence of the free natural product. The supernatant was discarded after being found to contain no natural product. The nanocomposites obtained were freeze-dried, weighed and stored for characterization, *in vitro* release and *in vivo* antimycobacterial studies.

Encapsulation Efficiency and Loading Capacity

The encapsulation efficiency (EE) of the nanomaterials is the total amount of the test bioactive chemical compound entrapped in the nanomaterials. The EE presented in the present study was computed by looking at the percentage of the ratio of amount of test compound in the nanomaterials to the initial total amount of the test compound (Equation (1)). On the other hand, the loading capacity (LC) of nanomaterials is the ability of the nanomaterials to entrap the test compound. The LC was determined by taking the percentage of the ratio of the amount of the active compound entrapped to the amount of the nanoformulation [Equation (2)] (Calvo et al. 1997, Vimal et al. 2012). The encapsulation procedure was conveyed out using 2 mg/mL and 0.1 mg/mL of chitosan and toussaintine A, respectively.

$$EE = \frac{\text{Total amount of Y - Free amount of Y}}{\text{Total amount of Y}} \times 100 \quad (1)$$

$$LC = \frac{\text{Total amount of Y - Free amount of Y}}{\text{Weight of the nanomaterials}} \times 100 \quad (2)$$

Where Y is the bioactive active compound understudy

***In Vitro* Release Studies**

The loaded chitosan nanoformulations (22 mg) containing 0.1012 mg of TA was suspended in a glass bottle containing 100 mL of the receiving medium at pH 7.4. The study medium constituted phosphate-buffered saline

(PBS) solution comprising 10% ethyl alcohol for solubility enhancement of the test compound (Nathiya et al. 2014). The resulting mixture was then stirred and incubated at 37 ˚C according to the established protocols in other literatures (Calvo et al. 1997, Mohammadpour et al. 2012). At specified time intervals (1, 2, 4, 6, 10, 22, 34, 48, and 72 hours), 5 mL of the taste sample was withdrawn from the receptor medium and centrifuged at 3500 rpm for 30 min while preserving the sink condition as previously reported elsewhere (Mohammadpour et al. 2012, Anbarasan 2013, Manikkam and Pitchai 2013). The freed quantity of the test compound in the supernatant was then assessed using UV-Vis spectrophotometer at 295 nm wavelength of maximum absorption and the cumulative percentage profile of *in vitro* release was plotted using equation 3.

$$\% \text{ Release} = \frac{\text{Released amount of Toussaintine A}}{\text{Initial Amount of Toussaintine A}} \text{ x } 100 \quad (3)$$

In Vivo Antimycobacterial Bioassay Study Using *Galleria Mellonella*

The MIP sub-culturing was carried out by adopting reported standard procedure (Erasto 2012, Rwegasila 2016). Inoculation of the sub-cultured MIP into the body of *G. mellonella* larvae was accomplished by interposing into the hemocoel through the last pro-leg. Bacterial inoculums were prepared from five-day grown cultures in Middlebrook 7H9 broth base containing 0.1% Tween 80, and the turbidity was adjusted to the equivalent of 0.5 McFarland units (approximately 1.2×10^8 CFU/mL). The injection was carried out by opening the last left pro-leg while gently applying pressure to the sides of the larva's body. The opening following injection was re- sealed off after the removal of the syringe, exhibiting absence of the damage. Incubation of the larvae was done at 37 °C while studying the effect of both free TA and TA-CS/TPP with respect to the controls. The *G. mellonella* larvae were thereafter observed after 24 and 48 h. To investigate the development of *MIP* in the larva's body, the G. *mellonella* larvae were dissected and the images were processed to evaluate the effect of the free TA and TA-CS/TPP nanocomposites.

Characterization of Materials

Infra-red (IR) spectra were recorded on the Alpha FTIR spectrometer from Bruker Optic GmgH, equipped with an ATR platinum crystal. The spectrometer was set to perform a total of 25 scans on each sample in the range of 500-4000 cm^{-1}. The absorption peaks generated during analysis were used for identification of the structural features of the materials and for the determination of degree of deacetylation (DD) of the prepared chitosan. The degree of deacetylation was determined in the previous study (Rwegasila et al. 2016). Absorption spectra were recorded on a Shimadzu UV/VIS-240 spectrophotometer in a range of 200 – 800 nm. The molecular weight of the purified chitosan was also determined in the previous study using MALDI-TOF-MS analysis (Rwegasila et al. 2016). Thus, tetrahydrofuran (THF) solution of the chitosan sample and trans-2-[3-(4-tert-butylphenyl)-2-methyl-2-propylidene] malononitrile (DCTB) matrix (1:10 v/v) was mixed in an Eppendorf tube. Then, 0.5 µL of the resulting solution was deposited on two spots on the stainless microtiter format MALDI target and dried at room temperature to produce a solid layer. The MALDI-TOF mass spectrum of chitosan was acquired by 500 laser shots by autoflex when the instrument was operating in the linear (flight path 1.22 m) mode with an acceleration voltage of 20.04 kV. The surface morphology analysis of chitosan, CS/TPP and TA-CS/TPP materials were performed by using a Zeiss Ultra plus FEG Scanning Electron Microscopy (SEM) and the LEO Ultra 55 SEM.

RESULTS AND DISCUSSION

IR Analysis

The infra-red spectrum of chitosan (Fig. 2) had a characteristic band at 3361 $cm^{-1}$for–NH_2 and –OH groups, 2925 cm^{-1} assigned to sp^3 C–H stretching vibrations, intense peak around 1555 cm^{-1} corresponding to the bending vibration of NH_2, 1151 cm^{-1} peak for the asymmetric stretch of C–O–C whereas peaks at 1651 and 1372 cm^{-1} were attributed to C=O and C–N stretching vibration as amide I and amide III of chitosan, respectively. The CS/TPP spectrum indicated a shifting of peak at 3361 cm^{-1} in pure CS to 3204 cm^{-1} in CS/TPP nanomaterial (Fig. 2) and broadened with decreased relative intensity at a ratio of 3:1 (A_{3361}/A_{3204}). The peak for the N-H bending vibration of amide II at 1555 cm^{-1} in CS shifted to 1535 cm^{-1} in CS/TPP nanomaterials with relative reduced intensity at approximately a 5:1 ratio (A_{1555}/A_{1535}), while the amide I C=O stretch observed at 1651 cm^{-1} in CS moved to 1625 cm^{-1} in CS/TPP. A new peak observed at 1214 cm^{-1} attributable to a P=O stretching vibration confirmed a cross-linkage (Rwegasila et al. 2016). A hypothetical representation of the interaction of toussaintia with CS/TPP is shown on figure 3.

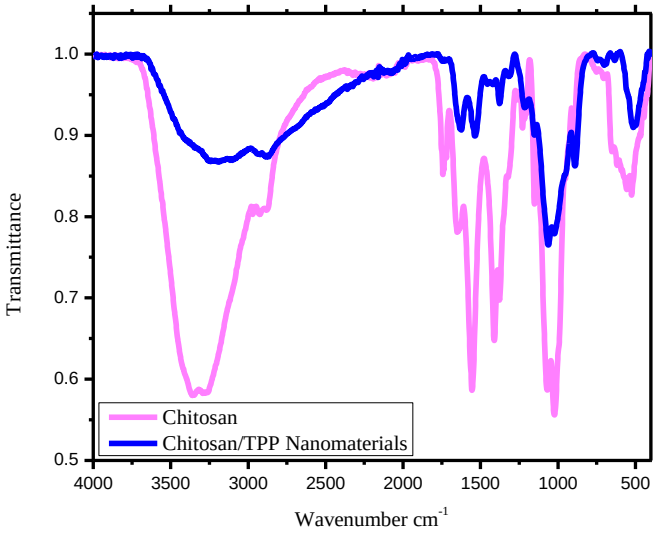

Figure 2: FTIR spectra of free CS and CS/TPP nanomaterials

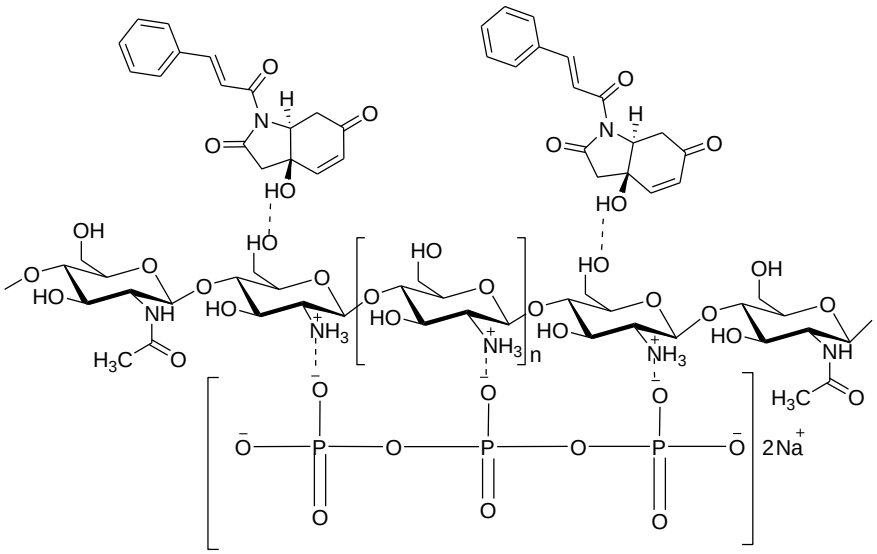

Figure 3: Hypothetical interactions between CS/TPP and TA

SEM Analysis

Scanning electron micrographs (SEM) of pure chitosan, CS/TPP and TA-CS/TPP are in Figure 4A-D. The SEM image of pure CS showed an uneven and rough surface with a spongy appearance (Fig. 4A). The rough surface of chitosan is due to low degree of deacetylation (Pandey and Khuller 2005**)**. Figure 4B shows SEM image of CS/TPP with non-uniform agglomerated particles with no clearly defined morphology. However, agglomeration increased when the TA was encapsulated, leading to the formation of a more compact non-uniform nanoformulation. This is evidenced by SEM image (Fig. 4C-D) showing that the particles were agglomerated with irregular shape, bumps and varying degrees of roughness. The agglomeration effect was influenced by the absence of stabilizing agent during loading and strong interaction due to inter- and intra-molecular hydrogen bonding (Nanda et al. 2012). The particle sizes of CS/TPP materials ranged from 1.128 to 200 µm while the diameters of TA-CS/TPP nanocomposites ranged from 0.359 to 12 µm. The strong interaction caused by inter- and intra-molecular hydrogen bonding between the TA and CS during the fabrication of CS/TPP-loaded nanocomposites might have accelerated to the observed reduced size of the agglomerated particles.

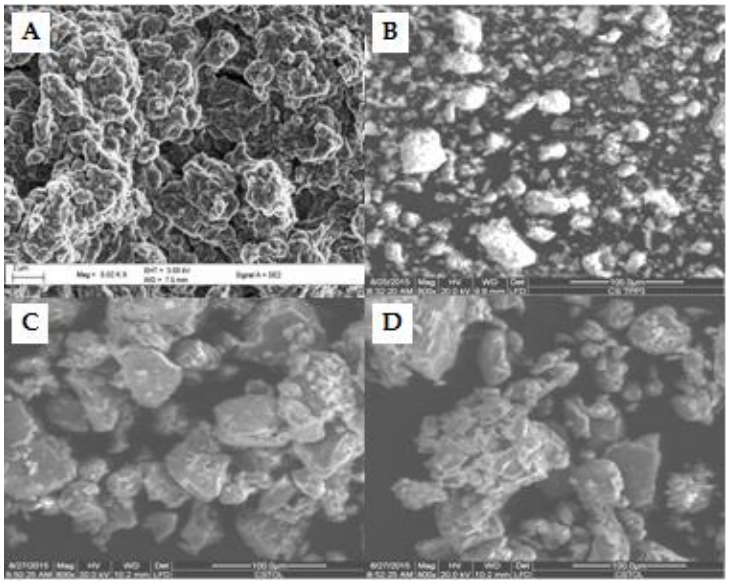

Figure 4: SEM images of (**A**) chitosan (scale bar = 2 µm); (**B**) CS/TPP (scale bar = 100 µm); (**C**) TA-CS/TPP (scale bar = 100 µm); and (**D**) TA-CS/TPP (scale bar = 100)

***In Vitro* Release Studies of the loaded TA**

The *in vitro* release profile of the loaded TA prepared using the 5:1 CS/TPP solution is showed in Figure 5. The release profile shows the initial burst of 27% of the TA after the first six hours. The initial higher release is anticipated to be due to the poorly-entrapment of TA during TA-CS/TPP nanofabrication. The study further indicated that 67% of TA was released within 72 h. The established burst release at 6 h (Fig. 5) could be desirable for the initial release of high amount of the bioactive compound for immediate and effective accessibility within 6 h.

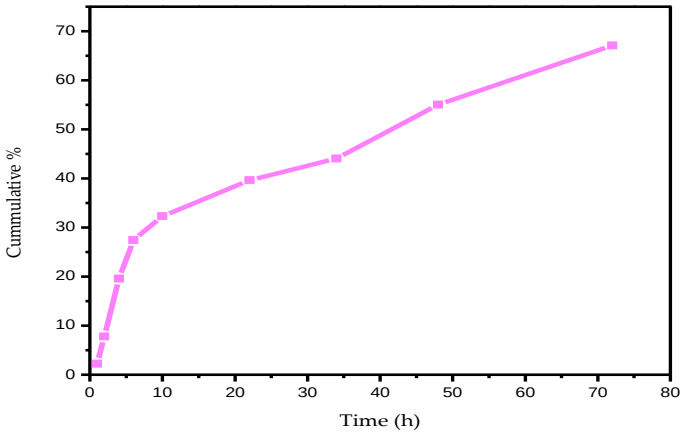

Figure 5: The release profiles of TA loaded to a 5:1 CS/TPP mass ratio.

In Vivo Antimycobacterial Assay

The results of *in vivo* antimycobacterial study are indicated in Table 1 in addition to Figures 6 and 7. The behaviors and effects of larvae treated with TA and TA-CS/TPP were observed by comparing with the controls after 24 and 48 h (Table 1 and Fig. 6). The positive control larvae were injected with *mycobacterium indicus pranii (MIP)* only, and the body immune system response versus the introduced bacteria was noted. The inoculated larvae turned into a black color after ten minutes, indicating the larval immune reaction due to cleavage of prophenoloxidase to activate phenoloxidase that limit the growth of *MIP* corresponding to the outcomes of other researchers (Cook and McArthur 2013). Following the aforementioned treatment, after 24 h of incubation at 37 °C, all of the positive control larvae died and appeared black colored (Table 1 and Fig. 6I). The death of positive control larvae resulted from inability of the body immune response to fight against the bacteria. This was contributed by extreme growth of bacterial colonies, which were of high density in the cells of the infected larva (Fig. 6L). However, the negative control larvae (Fig. 6J) were left free from bacteria and thus survived to the end of the study (48 h), indicating the absence of pathogenic infection as their cells appeared clean under the microscope (at the magnification of 100×) (Fig. 6M). The CS/TPP nanomaterials were also injected into the larvae in order to confirm their non-toxicity and it was observed that the larvae were well and active throughout the study (Table 1 and Figs. 6K, N).

In vivo antimycobacterial evaluations of TA and TA-CS/TPP showed a slight difference (Table 1 and Fig. 7) after monitoring the treated larvae for 24 h. However, a clear difference with remarkable effectiveness of encapsulated TA was found after 48 h. Clearance of bacterial colonies following the treatment was observed on dissecting the treated larvae which survived after 48 hours (Fig. 7A, B) when compared to the positive control (Fig. 6L) and negative control (Fig. 6M). The results showed that bacterial colonies in the treated larvae were cleared by 67% when free TA was applied to an *in vivo* system as visualized under the microscope (Fig. 7C). However, it should be noted that the dose of free TA tested higher compared to the amount of TA that was encapsulated on CS/TPP. The dose of loaded TA was simply 0.289 nM/mg bw compared to free TA, which was 90 nM/mg bw. Thus, TA-CS/TPP nanocomposites were more efficacious than the free TA. Consequently, considering the applied small dose of the loaded TA, these findings therefore, signify that utilization of CS nanoformulation can enhance the concentration of active compound at the target site compared to the free compound.

Table 1: *In vivo* antimycobacterial activity of *Mycobacterium indicus pranii* (MIP)-infected *Galleria mellonella* larvae.

Compound Dose	24 h		48 h	
	Dead (%)	**Alive (%)**	**Dead (%)**	**Alive (%)**
Free TA (90 nM/mg bw *)	17	83	33	67
TA -CS/TPP (0.289 nM/mg bw *)	20	80	40	60
CS/TPP	0	100	0	100

* bw = body weight

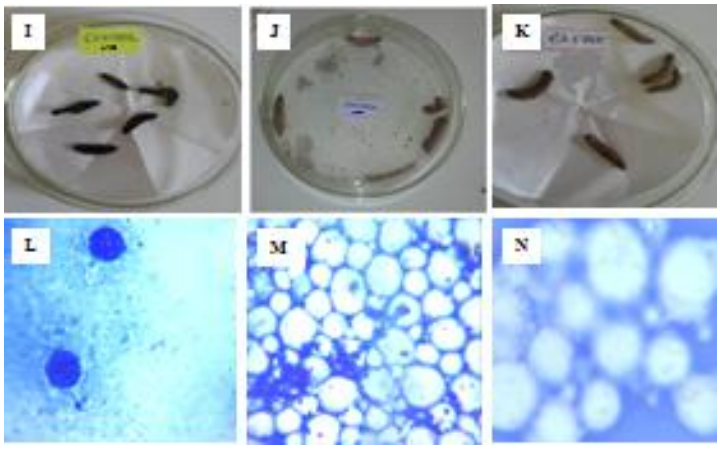

Figure 6: (**I**,**L**) Infected larvae (Positive control) and their appearance under the microscope at the magnification of 100×; (**J**, **M**) Non-infected Larvae (Negative control) and their appearance under the microscope at the magnification of 100×; (K, N) Larvae injected with Free CS/TPP and their appearance under the microscope at the magnification of 100×

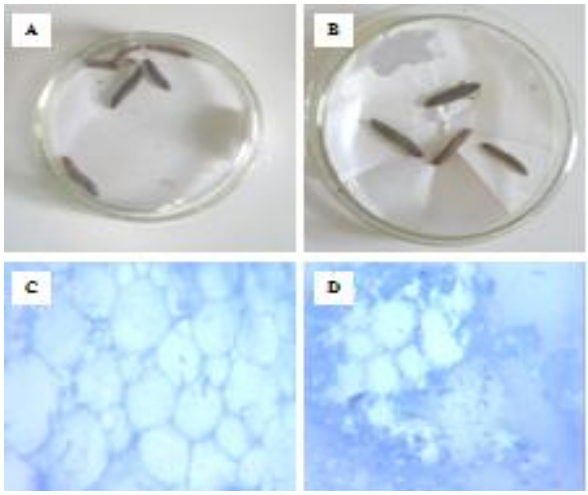

Figure 7: (**A**) Larva treated with the TA and their appearance under the microscope at the magnification of 100× (**C**); (**B**) Larva treated with the TA-CS/TPP nanocomposites and their appearance under the microscope at the magnification of 100× (**D**).

CONCLUSIONS

The encapsulated TA into the CS/TPP formulation was observed by the variation of surface morphology as revealed by SEM. The in vitro release profile of TA from the CS/TPP nano-framework was initially fast, up to 27% after the first six hours, then followed by a gradual release to the maximum of 67% after 72 h. The *in vivo* antimycobacterial activity of the free TA and the TA-CS/TPP

nanocomposites was comparable at 24 h with appreciable difference at 48 h, with encapsulated TA showing remarkable effectiveness at a very low dose concentration. Thus, the amount of the test compound in TA-CS/TPP nanocomposites injected into the larvae was indeed small, that is, 0.289 nM/mg bw compared to 90 nM/mg bw of the free TA. The present study therefore, concluded that the efficacy of TA is enhanced when encapsulated in the CS nanomaterials indicating that this approach improves bioavailability of natural products.

ACKNOWLEDGMENTS:
The study was supported by the International Foundation for Science (IFS) Grant No.J/5528-1. The authors are thankful to Aston University (UK), Gothenburg University (Sweden), Chalmers University of Science and Technology (Sweden), the University of Zululand (South Africa), the Institute of Traditional Medicine (Tanzania) and the National Institute for Medical Research, Ngongongare Medical Research Center, Arusha (Tanzania), for assistance with some of the analyses.

REFERENCES

Anbarasan B, Menon VV, Niranjana VA and Ramaprabhu S. 2013 Optimization of the formulation and in vitro evaluation of chloroquine loaded chitosan nanoparticles using ionic gelation method. *J. Chem. Pharm. Sci.* **6**:106–112.

Calvo P, Remunan-Lopez C, Vila-Jato JL and Alonso MJ. **1997** Novel hydrophilic chitosan–polyethylene oxide nanoparticles as protein carriers. *J. Appl. Polym. Sci.* **63**:125–132.

Cook SM and McArthur JD. 2013 Developing *Galleria mellonella* as a model host for human pathogens. *Med. Health Sci.* **4**:350–353.

Da Silva AL, Santos RS, Xisto DG, Alonso SV, Morales MM and Rocco PRM. 2013 Nanoparticle-based therapy for respiratory diseases. *Ann. Braz. Acad. Sci.* **85**: 137-146.

Deroin T and Luke QJ. 2005 A new Toussaintia (Annonaceae) from Tanzania. *East Afr. Nat. Hist.* **94**: 165-174.

Dhillon GS, Kaur S, Sarma SJ, Brar SK, Verma M and Surampalli RY. 2013 Recent Development in applications of important biopolymer chitosan in biomedicine, pharmaceuticals and personal care products. *Curr. Tissue Eng.* **2**: 20-40.

Erasto P. 2012 Antimycobacterial sterols from aromatic stem sap of *Commiphora eminii*. *Engl. J. Adv. Sci. Res.* **3**: 27–31.

Manikkam R and Pitchai D. 2013 Catechin loaded chitosan nanoparticles as a novel drug delivery system for cancer–synthesis and *in vitro* and *in vivo* characterization. *World J. Pharm. Pharm. Sci.*, **3**: 1553–1577.

Mohammadpour DN, Eskandari R, Avadi MR, Zolfagharian H, Mohammad SA and Rezayat M. 2012 Preparation and *in vitro* characterization of chitosan nanoparticles containing *Mesobuthus eupeus* scorpion venom as an antigen delivery system. *J. Venom. Anim. Toxins Incl. Trop. Dis.* **18**: 44–52.

Nanda RK, Patil SS and Navathar DA. 2012 Chiotsan nanoparticles loaded with thiocolchicoside. *Der Pharma Chemica*. **4**:1619-1625.

Nathiya S, Durga M and Devasena T. 2014 Preparation, physico-chemical characterization and biocompatibility evaluation of quercetin loaded chitosan nanoparticles and its novel potential to ameliorate Monocrotophos induced toxicity. *Digest. J. Nanomater. Biostruct.* **9**:1603–1614.

Nyandoro SS. 2014 Some Rare Tanzanian Plant Species as Sources of less Common Metabolites: Biomedical Potential and Conservation Status. *J. Pharmacogn. Phytochem*. **3**:147-157.

Nyandoro SS, Ndanu J, Munissi JJE, Gruhonjic A, Fitzpatrick PA, Landberg G, Lu Y, Wang, B, Pan F, Rissanen K and Erdélyi M . 2015 N-Cinnamoyltetraketide derivatives from the leaves of *Toussaintia orientalis*. *J. Nat. Prod*. **78**: 2045–2050.

Pandey R and Khuller GK. 2005 Solid lipid particle-based inhalable sustained drug delivery system against experimental tuberculosis. *Tuberculosis*. **85**: 227–234.

Ranjita S, Loaye A and Khalil M. 2011 Present Status of Nanoparticle Research for Treatment of Tuberculosis. *J. Pharmaceut. Sci*. **14**:100–116.

Rwegasila E, Mubofu EB, Nyandoro SS, Erasto P and Munissi JJE. 2016 Preparation, characterization and *in vivo* antimycobacterial studies of panchovillin-chitosan nanocomposites. *Int. J. Mol, Sci.* **17**:1-16.

Samwel S, Odalo JO, Nkunya MHH, Joseph, CC, Koorbanally, NA 2011 Toussaintines A–E: Antimicrobial indolidinoids, a cinnamoylhydrobenzofuranoid and a cinnamoylcyclohexenoid from *Toussaintia orientalis* leaves, *Phytochemistry* **72**:1826 – 1832.

Tiyaboonchai W. 2003 Chitosan Nanoparticles: A Promising System for Drug Delivery. *J. Naresuan. Univ*. **11**: 51-66.

Vimal S, Majeed S.A, Taju G, Nambi KSN, Raj NS, Madan N, Farook MA, Rajkumar T, Gopinath D and Hameed ASS. 2013 Chitosan tripolyphosphate (CS/TPP) nanoparticles: Preparation, characterization and application for gene delivery in shrimp. *Acta Trop.* **128**: 486–493.

World Health Organization. Global Tuberculosis Report. 2013. Available online: http://www.who.int/iris/bitstream/10665/91355/1/9789241564656_eng.pdf (accessed on 1 April 2015).

Zhang Y, Yang Y, Tang K, Hu X and Zou G. 2008 Physicochemical Characterization and Antioxidant Activity of Quercetin-Loaded Chitosan Nanoparticles. *J. App. Poly. Sci.* **107**: 891–897.